



Contents lists available at ScienceDirect

Remote Sensing of Environment

journal homepage: www.elsevier.com/locate/rse

Hyperspectral discrimination of floating mats of seagrass wrack and the macroalgae *Sargassum* in coastal waters of Greater Florida Bay using airborne remote sensing

H.M. Dierssen^{*}, A. Chlus, B. Russell

Department of Marine Sciences, University of Connecticut, Groton, CT 06340, USA

ARTICLE INFO

Article history:

Received 7 July 2014

Received in revised form 12 January 2015

Accepted 27 January 2015

Available online xxxxx

Keywords:

Floating algae

Seagrass

Wrack

Remote sensing

Hyperspectral

Langmuir

*Sargassum**Syringodium filiforme*

Airborne imaging spectroscopy

Beach wrack

Ocean color

PRISM

ABSTRACT

Floating mats of vegetation serve to transfer biomass, nutrients and energy across marine habitats and alter the spectral properties of the sea surface. Here, spectral measurements from the airborne Portable Remote Imaging Spectrometer (PRISM) imagery at 1-m resolution and experimental mesocosms were used to assess the hyperspectral properties of the macroalgae *Sargassum* and aggregations of the seagrass *Syringodium filiforme* wrack in Greater Florida Bay. A simple Normalized Difference Vegetative Index (NDVI) effectively discriminated the presence of vegetation floating on the sea surface. The Sargassum Index derived from reflectance ratios at 650 and 630 nm was used to effectively discriminate *Sargassum* from *Syringodium* wrack. Mesocosm spectral measurements revealed an initial lowering of wrack reflectance over the first 3 days followed by a subsequent increase in reflectance over the next 8 days. The age of the wrack estimated from 2 to 5 days was best characterized using narrowband indices of the water absorption feature at 930 and 990 nm potentially from increasing water content in wrack leaves over time. Hyperspectral imagery (<10 nm) was necessary to differentiate between these two types of floating vegetation and assess age of the wrack. PRISM imagery revealed seagrass wrack organized in 5–35 m spaced windrows caused by Langmuir circulation. Wrack was only detectable at 60 m pixel resolution when densities were high and individual windrows were in close proximity.

© 2015 Elsevier Inc. All rights reserved.

1. Introduction

Floating mats of vegetation are a widespread but ephemeral feature in the world ocean that serves to transfer biomass, nutrients, and energy across marine and coastal habitats (Heck et al., 2008). The Sargasso Sea, for example, is broadly defined by the presence of mats of the eponymous drifting macroalgae *Sargassum*. The high turnover of buoyant leaves from submerged seagrass meadows can also produce large cohesive aggregations of floating vegetation called seagrass wracks. The extent of different types of floating marine vegetation is not well constrained and new methods are required to assess the associated ecological and economic implications. Traditional remote sensing methods can be used to identify the presence or absence of large mats of floating vegetation (Cavanaugh, Siegel, Kinlan, & Reed, 2010; Gower, Hu, Borstad, & King, 2006; Hu, 2009). Airborne hyperspectral and thermal infrared imagery has also been used to evaluate *Sargassum* rafts along the Florida Current (Marmorino, Miller, Smith, & Bowles, 2011), but the potential to spectrally discriminate

between different types of floating vegetation using remote sensing imagery has yet to be determined.

Vegetative mats have both ecological and economic significance. *Sargassum* mats in particular have a well-studied endemic faunal community. The mats and associated fauna are an important source of structure and food in the open ocean for fish, birds, turtles, and invertebrates. Over 100 fish species are known to utilize the mats during some portion of their life cycle, with many utilizing the algae as juveniles. Recognized by the South Atlantic Fishery Management Council as Essential Fish Habitat (Connolly, 2002), *Sargassum* is associated with commercially and recreationally important fish species like mahi, snapper, and grouper (Coston-Clements & Center, 1991). Seagrass and associated leaf and stem debris also support diverse epiphytic populations of autotrophic algae (Frankovich, Armitage, Wachnicka, Gaiser, & Fourqurean, 2009). When washed ashore, vegetative wrack may serve as trophic subsidy providing breeding habitat for terrestrial insects and foraging space for shore birds (Dugan, Hubbard, McCrary, & Pierson, 2003; Ince, Hyndes, Lavery, & Vanderklift, 2007). New studies are suggesting that marine deposited wrack may impact terrestrial ecosystems further inland than previously thought (Mellbrand, Lavery, Hyndes, & Hambäck, 2011).

Wrack can also negatively impact the growth of salt marshes (Macreadie, Hughes, & Kimbro, 2013) and public use of the shoreline.

^{*} Corresponding author at: Department of Marine Sciences, University of Connecticut Avery Point, 1080 Shennecossett Road, Groton, CT 06340-6048.
E-mail address: heidi.dierssen@uconn.edu (H.M. Dierssen).

In large enough quantities, wrack can prevent human access to beaches and are hotspots of organic carbon degradation that can potentially flux gases such as hydrogen sulfide and methane into the atmosphere (Oldham, Lavery, McMahon, Pattiaratchi, & Chiffings, 2010). Mass landings can last several weeks, and be detrimental to economies that rely on tourism and recreation. Coastal Texas, for example spends considerable effort on clearing algal wrack from important coastal areas. A *Sargassum* Early Advisory System provides warnings to Texas coastal managers when a large pulse of *Sargassum* is likely to cause beach closures (Webster & Linton, 2013). Indeed large scale deposition of seagrass wrack and macroalgae along coastlines has been the subject of intensive global research, management, and education programs from Australia to the German Baltic coastline (Lavery, McMahon, Weyers, Boyce, & Oldham, 2013; Mossbauer, Haller, Dahlke, & Schernewski, 2012).

Remote sensing represents a useful approach for measuring the extent, movement, and distribution of floating vegetation in marine and inland waters. The capability of distinguishing between types of vegetation (seagrass wracks, *Sargassum*, kelp), however, may be limited using multi-spectral sensors. Previous work detecting *Sargassum* with ocean color imagery (Gower, King, Borstad, & Brown, 2008; Gower et al., 2006), for example, utilized the “red edge” of surface chlorophyll with information from sensor bands at 681, 709, and 754 nm (MERIS) and 665.1, 676.7, and 746.3 nm (MODIS). The Floating Algae Index uses a similar approach but with bands further out into the infrared (865 nm) and shortwave (1240 or 1660 nm) to minimize problems with atmospheric correction (Hu, 2009). Because all vegetative matter exhibits a red edge of reflectance, such techniques will not necessarily differentiate the composition of floating vegetation. The reflectance spectrum of different types of vegetated matter at the sea surface will vary with the suite of photosynthetic pigments, age and physiological state of the biomass, degree of submersion and optical properties of the water column.

Floating vegetation is not homogenous across the sea surface and the patchy distribution can be readily assessed using remote sensing techniques. Biomass aggregates along different currents and circulation features of surface water masses. Hydrographic fronts occur at adjoining water masses of different densities. Downwelling fronts in the Gulf Stream, in particular, have been known to accumulate organisms ranging from zooplankton to seabirds (Haney & McGillivray, 1985; Herron, Leming, & Li, 1989; Witherington, 2002). Downwelling can also be set up by winds that produce a spiraling circulation caused by Langmuir circulation (Thorpe, 2004). Both benthic and surface windrows can be found in coastal waters with the rows running parallel to the prevailing wind direction (Dierssen, Zimmerman & Burdige, 2009; Dierssen, Zimmerman, Drake & Burdige, 2009).

Here, spectroscopy is used in the laboratory and from the airborne Portable Remote Imaging Spectrometer (PRISM) (Mouroulis et al., 2013) to assess the spatial distribution and hyperspectral properties of seagrass wrack and *Sargassum* in Greater Florida Bay. We also present remote sensing algorithms to discriminate between the two types of vegetation and the potential age of the seagrass wrack. An analysis is conducted to determine the spatial resolution at which the fine-scale distributions of seagrass leaves can be detected from remote sensing imagery. These data serve as an analog to future satellite assets, like the proposed HypSPIRI sensor, that will have full spectral capabilities with higher spatial resolution than most ocean color satellites.

2. Methods

2.1. Study site

This study was conducted in January 2014 in the Greater Florida Bay region with facilities provided by Keys Marine Laboratory in Long Key, FL, USA (24°49.55'N, 80°48.85'W). The shallow estuarine watershed extending south of the Florida peninsula out to the Florida Keys is referred

to as Greater Florida Bay and is influenced by fresh water from the everglades mixed with the salty waters from the Gulf of Mexico. The region contains extensive seagrass meadows covering over 14,000 km² (Fourqurean et al., 2001). Dense seagrass beds consisting primarily of the cylindrical-bladed manatee grass *Syringodium filiforme* extend approximately 10 km to the northwest of Long Key (Fig. 1). These shallow meadows occur in 2–3 m water depth with a 0.5 m canopy height and shoot densities up to 2500 shoot m⁻² (McPherson, Hill, Zimmerman, & Dierssen, 2011). Locations sampled within the Greater Florida Bay are termed “bayside.” Flow on the bayside is tidally driven with high particulate scattering over regions comprised of sandy bottoms (McPherson et al., 2011).

The continental shelf to the south of the Keys is approximately 5–15 m in depth and contains mixtures of sand, coral reefs and moderate stands of turtlegrass, *Thalassia testudinum*. The shoreward edge of the Gulf Stream runs along the shelf south of the Keys flowing from southwest to northeast. Water is more oligotrophic with lower absorption and scattering coefficients compared to bayside stations (McPherson et al., 2011). Sampling locations along the shelf south of Long Key are termed “oceanside.” Research in the Florida Keys National Marine Sanctuary was conducted under NOAA permit (FKNMS-2010-151) and a Special Activity License through the Florida Fish & Wildlife Conservation Commission (SAL-10-1274A-SR).

2.2. Hyperspectral imagery

Imagery was collected using the Portable Remote Imaging Spectrometer (PRISM), a push broom hyperspectral imager designed specifically for coastal applications (Mouroulis, Green, & Wilson, 2008). PRISM is equipped with two sensors, a visible-near infrared (NIR) imager with a spectral range of 350–1050 nm and spectral resolution of 3.1 nm and shortwave infrared spot radiometer which records data in two bands, 1240 nm and 1610 nm at a spectral resolution of 20 nm, to aid in atmospheric correction.

Flight lines over floating rafts of *Syringodium* wrack and *Sargassum* were flown aboard a DHC-6 Twin Otter between 13 and 19 January 2014 at altitudes of 900 m and 3000 m, resulting in spatial resolutions of approximately 0.9 m and 2.7 m respectively (Fig. 1C). Three passive Lagrangian surface drifters were deployed simultaneously over the dense *Syringodium* meadows bayside to track flow of drifting vegetation during the PRISM overflights. A single deployment lasted from 11 January until the drifters ran aground along Long Key on 16 January 2014 (Fig. 1B). The drifters tracked the upper meter of the water column (with some wind drag) and contained GPS transmitters that broadcast their position every half hour (<http://www.neracoos.org/drifters>).

PRISM imagery was atmospherically corrected using a modified version of the ATREM radiative transfer model to account for Rayleigh scattering, background aerosol scattering and absorption effects from atmospheric gases (Gao & Davis, 1997). Because individual wave facets were resolved in the meter-scale imagery, traditional sun glint corrections could not be applied. In order to remove these residual effects, a mask was developed using PRISM channels centered near 660 and 860 nm to differentiate land and floating vegetation pixels from water pixels without floating vegetation. Residual sun glint was assumed to be spectrally constant and set equal to the Rayleigh-corrected reflectance at 980 nm (where the water leaving reflectance is close to zero). For each water pixel without significant floating vegetation, this constant glint value was subtracted from the Rayleigh-corrected reflectance spectrum at all wavebands (Mouroulis et al., 2013). Comparisons of the PRISM imagery with seagrass wrack spectra collected coincidentally in the harbor showed that the atmospheric correction was generally accurate across the visible and NIR (Fig. 2). The small noise in the PRISM imagery is primarily due to errors in the standard solar irradiance curve at high spectral resolution. Errors in UV wavelengths are associated with lamp calibration limitations and data are truncated at wavelengths less than 380 nm.

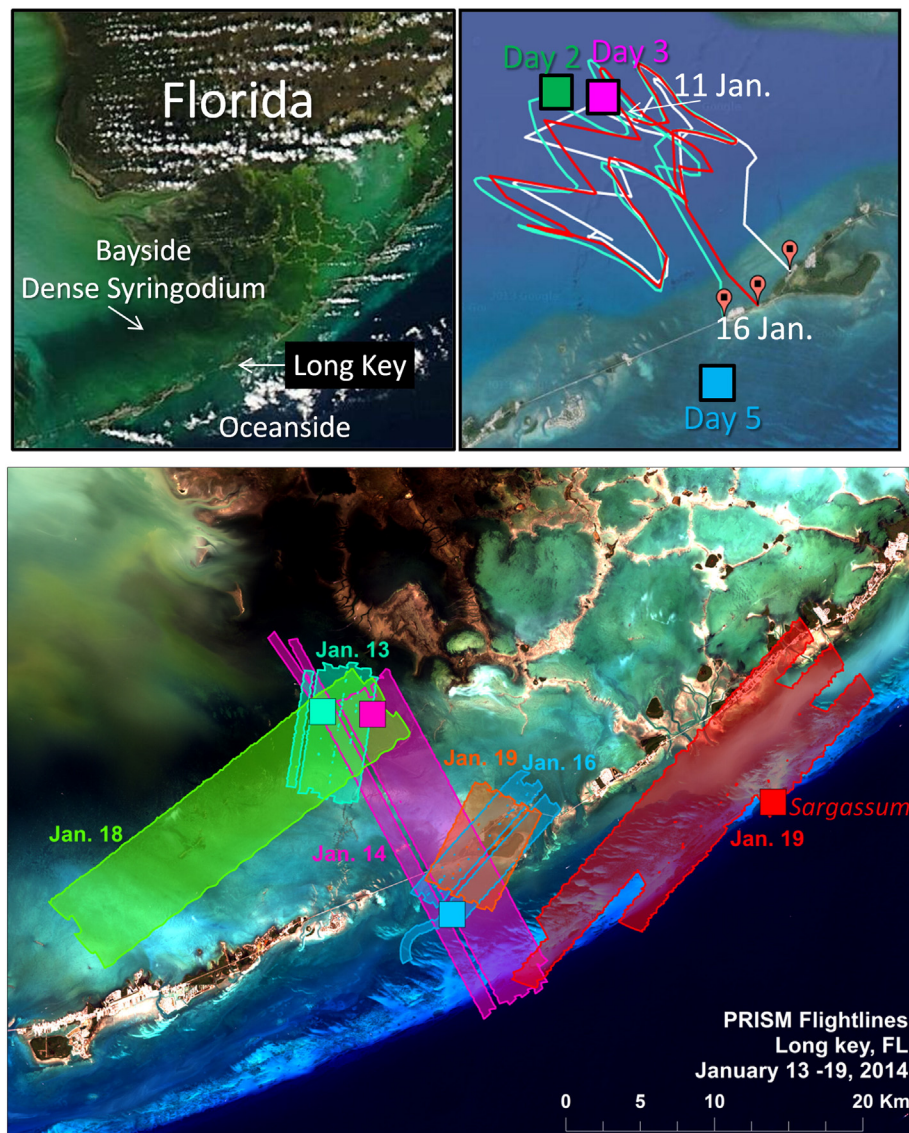


Fig. 1. A) The study location in Greater Florida Bay is indicated by a MODIS pseudo-true color image of the region. B) Drifter locations of three buoys deployed over the dense *Syringodium* beds identified in panel A from 11 January to when they ran aground on Long Key on 16 January 2014. C) Daily overflight tracks taken with the Portable Remote Imaging Spectrometer (PRISM) during the field campaign. The colored squares correspond to the flight days and indicate the regions of floating *Syringodium* wrack (pink, blue and green) and *Sargassum* (red) highlighted in this study.

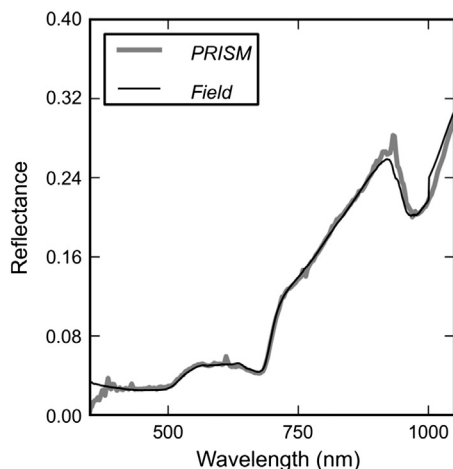


Fig. 2. Comparison of atmospherically corrected PRISM imagery with coincident field spectrum taken over *Syringodium* wrack present in the harbor on Long Key, Florida.

2.3. Spectral sampling of floating vegetation

Samples of floating *Syringodium* leaf and stem debris were collected over seagrass beds between 06 and 09 January, 2014 and placed into mesocosms at Keys Marine Laboratory. Mesocosms were long tanks filled with running filtered seawater pumped from the harbor that were open to the air and incident sunlight. Daily spectral measurements were made using a FieldSpec 4 wide-res spectroradiometer (ASD Inc.) with a 8.5° field of view foreoptic. The FieldSpec 4 has a spectral range of 350–2500 nm with a spectral resolution of 3 nm in the range 350–1400 nm and 30 nm from 1400–2500 nm. Spectral measurements were collected between 09:00 and 16:00 local time when weather and solar conditions allowed. Field spectroscopy was conducted in air on samples briefly removed from the mesocosm to determine the reflectance of the biomass itself without variability induced by the concentration of floating material, degree of submergence, and amount of background water. Samples were placed on a piece of black cloth and arranged in dense aggregations to eliminate the influence of background spectra. Five spectral measurements on different parts of

the sample from the downward facing probe at a height of 15 cm were recorded for each sample. Spectra were referenced to radiance measurements from a 99% white Spectralon panel (Labsphere Inc.) placed adjacent to the sample. Spectral Reflectance, $R(\lambda)$, represents the amount of light reflecting from the sample at a given wavelength, λ , divided by the amount reflecting off of the Spectralon panel.

Samples of *Sargassum* were also collected throughout the course of the field campaign and spectral measurements were taken using the procedures described above. In situ measurements of the wrack and *Sargassum* floating in water were also taken from a small boat using the same spectrometer and calibrating against a Spectralon panel. A 45° angle to the water was used to minimize sun glint and the measurement was taken at roughly 135° azimuth from the sun (Moble, 1999).

2.4. Data analysis

Images were spectrally resampled to spectral properties ranging from 380–1050 nm and 10 nm resolution using ENVI (Exelis Visual Information Systems). A coarser spectral resolution was used to provide an analog for potential future hyperspectral satellite missions such as the proposed HypSPIRI sensor. ENVI uses a Gaussian curve to model the spectral response of the target sensor using the band center and spectral resolution to define the curve. Features including narrowband indices, red edge position, spectral slopes and continuum removed absorption bands were assessed for their utility in discriminating between seagrass debris and floating macroalgae, e.g., (Mutanga & Skidmore, 2004).

Pixels containing floating vegetation were isolated using the Normalized Difference Vegetation Index (NDVI) (Tucker, 1979). NDVI, which contrasts the reflectance in the NIR to red reflectance, has been used to detect floating algae (Hu & He, 2008) and similar detection results were achieved for floating seagrass wrack. Positive NDVI values characteristic of vegetation provided a strong contrast to surrounding water which has NDVI values that are typically less than 0 due to strong absorption of NIR radiation. A threshold NDVI value of 0 was used to mask water pixels and a threshold of 1% NIR reflectance was used to identify pixels containing detectable types of floating vegetation.

Narrowband indices were evaluated on the spectra of differently aged *Syringodium* wrack as measured in the mesocosm experiments (Mutanga & Skidmore, 2004). A modified version of NDVI, ($NDVI_m$, Eq. 1) was calculated for all pairwise combinations of reflectance in

bands within the HypSPIRI spectral range (380–2500 nm, 213 bands) which resulted in 22,684 spectral indices.

$$NDVI_m = \frac{R(\lambda_1) - R(\lambda_2)}{R(\lambda_1) + R(\lambda_2)} \quad (1)$$

The relationship between wrack age and $NDVI_m$ for each band combination was assessed using linear regression and discussed in Section 3.2.

3. Results

On January 11, drifter buoys were deployed over the dense seagrass beds north of Long Key during low to moderate wind conditions. No apparent aggregations of seagrass wrack were observed at that time. Over the next few days, the winds remained moderate to low ($<8 \text{ m s}^{-1}$) and the drifter buoys fluctuated within the bay following the tidal cycle (Fig. 1B). During this time two patches of drifting vegetation were detected in the PRISM imagery on 13 and 14 January. As there were no new wind events, we presume that the vegetation aggregated in the imagery reflected biomass that was at least 2 and 3 days old. On the 16 January, high southward moving winds developed ($>10 \text{ m s}^{-1}$) and the buoys tracked southward with the winds until they ran aground on Long Key. Organized windrows of vegetation were then observed oceanside just south of Long Key (Fig. 3A). We speculate that this floating vegetation was at least 5 days old and was recently advected oceanside with the strong winds. The imagery revealed floating vegetation organized into rows approximately 30–35 m in spacing (Fig. 3A). While not observed coincidentally with the imagery, large aggregations of *Syringodium* wrack were advected oceanside during an earlier wind event on 7 January that coincided with $>10 \text{ m s}^{-1}$ winds in a southerly direction (Fig. 3B).

During our field investigations, $>97\%$ of the observed floating vegetation was *Syringodium* leaf and stem debris. During the last day of overflights on 19 January, vegetation was detected in the PRISM imagery floating oceanside off the continental shelf (red square in Fig. 1C). As described below, the spectral signature was consistent with field measurements of *Sargassum*. The following results outline methods for using remote sensing techniques to discriminate between these two types of floating vegetation detected with the PRISM imagery and to potentially derive the age of the floating seagrass wrack.

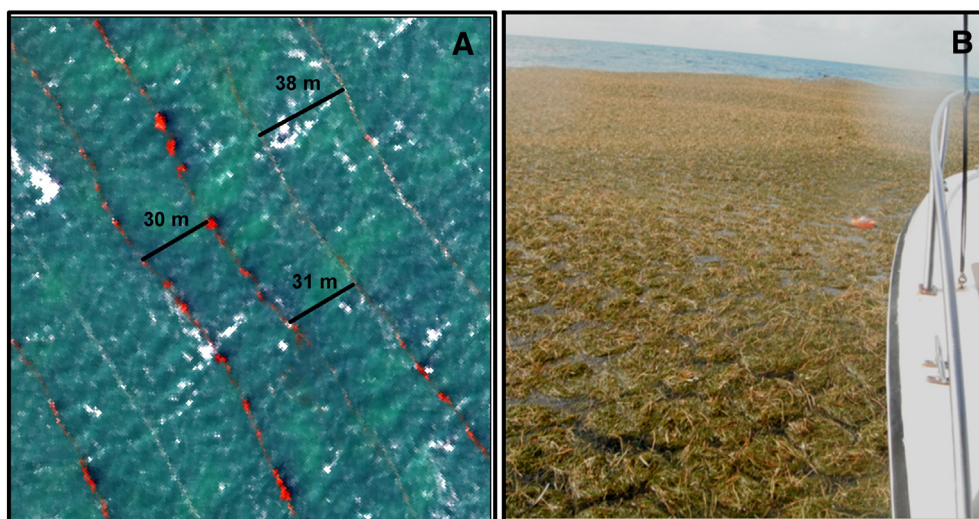


Fig. 3. A) A pseudo-true color image highlighting the floating seagrass wrack aggregated into windrows on the oceanside 16 Jan. 2014. B) A photograph taken from a boat oceanside of the drifter buoy (orange) in a large aggregation of seagrass wrack with individual whorled structure on 10 Jan. 2014 (photo credit R. Perry).

3.1. Methods for spectral discrimination of vegetation

Spectral signatures of *Syringodium* wrack and *Sargassum* obtained in the field and from our mesocosms show patterns that are typical of vegetation: strong absorption between 650 nm and 685 nm with a minimum at 675 nm caused by photosynthetic pigments and high reflectance in the NIR attributed to internal tissue structure (Gitelson & Merzlyak, 1994) (Fig. 4). The red edge of reflectance is common in all vegetation, including concentrated dense aggregations of phytoplankton (Dierssen, Kudela, Ryan, & Zimmerman, 2006), but not often observable in oceanic conditions due to high red and NIR absorption by water molecules. Reflectance measured on the mesocosm samples was conducted with dense clumps of vegetation removed from the water. These samples, referred to as “Out of water” (Fig. 4), revealed similar patterns in visible wavelengths (400–700 nm) but considerably higher NIR reflectance (>700 nm) than those obtained from vegetation floating at the air–water interface (“In water”).

Spectral differences were observed between these two types of vegetation that could be used to uniquely identify their presence on the sea surface using hyperspectral data. *Sargassum* is a genus of brown macroalgae (Phaeophyceae) that contains accessory pigments fucoxanthin and chlorophyll *c* (Johnsen & Sakshaug, 2007). The in vivo absorption peaks for fucoxanthin occur in the blue and green wavelengths with peaks at 480 and 520 nm. Absorption peaks for chlorophyll *c* occur at 460, 485, and 635 nm (Grzymiski, Johnsen, & Sakshaug, 1997).

In contrast, seagrasses are flowering plants (angiosperms) and their leaves lack accessory pigments that permit efficient harvesting of green light (Cummins & Zimmerman, 2003). However, seagrass leaves contain chlorophyll *b* which has absorption peaks in blue and red wavelengths corresponding to 470, 600, 650 nm. These specific absorption bands can create local minima in the reflectance spectra.

The reflectance spectra from the two types of floating vegetation show distinct differences that can be attributed to these differences in accessory pigments (Fig. 5A). *Syringodium* wrack had higher reflectance

in the green wavelengths (500–600 nm) due to the lack of accessory pigment absorption and low reflectance at 650 nm which coincides with chlorophyll *b* pigment absorption. In contrast, the *Sargassum* spectrum contains a distinct dip at 630 nm not present in *Syringodium*. This feature is not due to fucoxanthin, as reported in a prior study (Szekielda, Marmorino, Bowles, & Gillis, 2010), but due to chlorophyll *c* absorption at 630–635 nm (Beach, Borgeas, Nishimura, & Smith, 1997; Grzymiski et al., 1997) (Fig. 5A). Using a simple ratio (Jordan, 1969), a narrowband index was developed to distinguish between the two classes of floating vegetation. The *Sargassum* Index (SI) uses reflectance values at 650 nm and 630 nm (Eq. 2) to differentiate *Sargassum* from seagrass wrack and other floating vegetation that do not contain this 630 nm absorption feature:

$$\text{Sargassum Index} = \frac{R(650)}{R(630)} \quad (2)$$

Distributions in SI values (Fig. 5B) from pixels identified in the PRISM imagery show a distinct difference between vegetation types. *Sargassum* was found to have values typically greater than 1.0 indicating the low reflectance at 630 nm attributable to chlorophyll *c*; whereas, SI values of *Syringodium* wrack were generally less than 1 with more reflectance at 630 than 650 nm.

At Day 5, *Syringodium* wrack showed a shift in SI values towards zero (Fig. 5B). This change is believed to be the result of typical leaf senescence and epiphytic algal growth on the seagrass increasing absorption in the range 650–700 nm. Hence, seagrass wrack became more separable from *Sargassum* as it aged. Additional variables tested for discrimination including NDVI, red edge position and red edge slope, did not show significant differences between types. The basic algorithm for differentiating floating vegetation using the PRISM imagery and potentially other hyperspectral sensors is outlined in Fig. 6.

3.2. Spectral trends of decaying seagrass debris

Results of the mesocosm experiments were used to assess changes in the spectral signatures of seagrass wrack over time. While some fraction of the wrack lost buoyancy and sunk to the bottom of the mesocosm each day, a portion of the wrack remained floating throughout the duration of the 12-day experiment. Floating wrack sampled near daily from the mesocosm showed a unique and changing spectral reflectance pattern with age. Over the first 3 to 4 days in the mesocosm, a general decline was observed in the magnitude of reflectance in the visible through NIR spectrum with lower apparent absorption at 664 nm and flatter visible reflectance (Fig. 7). This pattern reversed over the remainder of the experiment and a continual increase in reflectance was observed over the next 8 days. The spectral dip at 664 nm, which initially decreased over the first 3–4 days, subsequently increased towards the end of the experiment.

The mesocosm spectra for each day shown in Fig. 7 were averages of five measurements distributed haphazardly across the wrack sample. The duplicate measurements conducted each day clearly revealed the general decreasing pattern in average reflectance (380 to 1400 nm) over the first four days followed by an increasing reflectance over time (Fig. 8). These measurements illustrate how the standard deviation for each sample increased towards the end of the experiment. Reflectance of the wrack made on the day it was collected (Day 0), for example, varied less than 8% across the five replicates. On Day 12, the sampled spectra spanned over 20% in spectral range from 0.18 to nearly 0.38. This suggests that the wrack did not age uniformly across individual leaves and stems.

Pairwise index analysis of $NDVI_m$ conducted on the wrack mesocosm spectra from Fig. 7 revealed several spectral regions that were correlated to debris age (Fig. 9). The area of greatest correlation centered around the band combination 990 nm and 930 nm, where the correlation coefficient (R^2) equaled 0.68. This spectral region, shown as red in Fig. 9A, contains the top 24 band pairs with the highest correlation coefficients

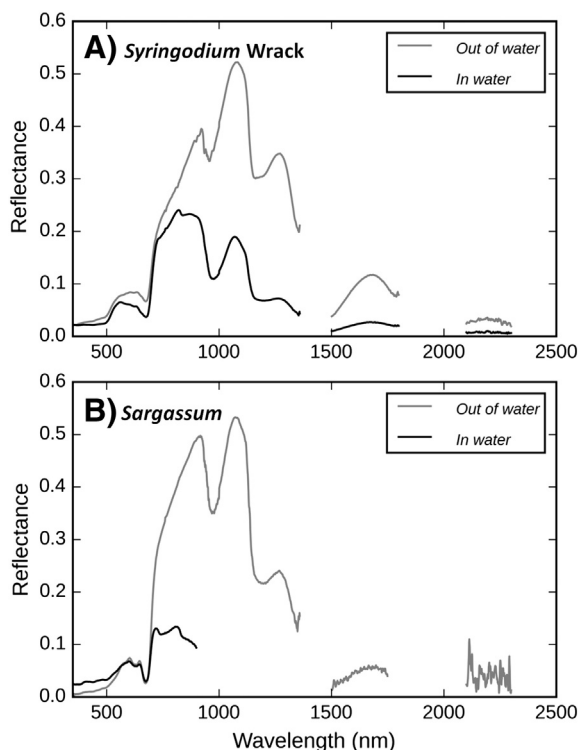


Fig. 4. Reflectance measurements taken of floating vegetation in natural habitat (“In water”) and removed from water during the mesocosm experiments (“Out of water”) of: A) seagrass leaf and stem debris, *Syringodium* wrack; and B) the macroalgae *Sargassum*. In water measurements of *Sargassum* only extend to 900 nm.

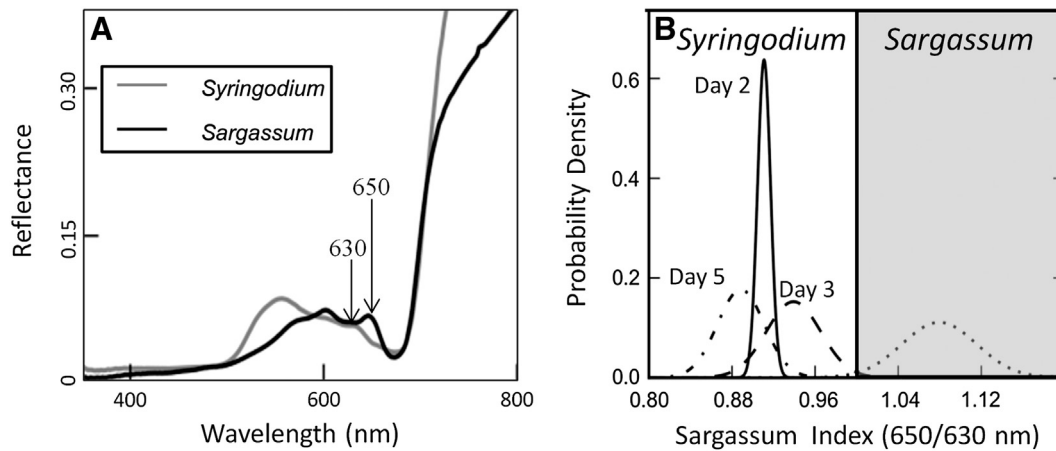


Fig. 5. A) Differences in reflectance spectra derived from the PRISM instrument revealing the unique spectral absorption feature in *Sargassum* not observed in *Syringodium* wrack. B) Results of the Sargassum Index algorithm revealing *Sargassum* pixels with a value greater than 1 and *Syringodium* wrack of different ages with values less than 1.

(Mean = 0.59). This absorption band is known to be indicative of vegetation water content and water stress (Claudio et al., 2006; Peñuelas, Pinol, Ogaya, & Filella, 1997) and suggests changes in water content within the wrack with age (Fig. 9B). The second highest band pair region is centered at 1300 nm and 1200 nm where $R^2 = 0.51$. Reflectance at 1200 nm is also used for monitoring plant canopy water content (Claudio et al., 2006). An additional pair with a significant correlation coefficient is the combination of bands 670 nm and 660 nm, a region associated with chlorophyll absorption. The striped patterns in the short wave infrared are due to low signal to noise in this part of the spectrum.

Wrack identified in the PRISM imagery showed similar trends in spectral shape as those measured in the mesocosm (Fig. 10A). Consistent with 3–4 day old wrack from the mesocosm, the PRISM spectra assessed as Day 3 wrack (based on sampling time and coincident buoy data) had a flatter spectrum throughout the visible wavelengths. Wrack from Day 5 contained a slightly higher NIR signal and a more pronounced chlorophyll absorption dip compared to Day 3. Visually

assessed, such a pattern could be similar to mesocosm wrack from Day 0 or greater than Day 4. Calculations of the $NDVI_m$ using 990 and 930 nm wavelengths were conducted to determine whether narrow-band features could elucidate the age of the PRISM wrack. As shown in Fig. 10B, both the mesocosm and PRISM measurements showed similar negative trends with age but a substantial offset existed between the two lines. This offset may be due to differences in sampling; mesocosm measurements were conducted in air and the PRISM measurements were conducted over water. Moreover, atmospheric correction of the PRISM imagery used the 980 nm waveband and may have removed some of the leaf signal as sea surface glint. The similar negative trend in the $NDVI$ value, however, was consistent with the drifter-determined age assessments and provided further evidence that the oceanside wrack (Day 5) was older than the bayside wrack (Day 3).

3.3. Distribution and abundance estimates

After designating PRISM pixels as potentially containing seagrass, a linear unmixing model was used to estimate percent cover of seagrass debris in the PRISM imagery. Endmembers were selected using the Sequential Maximum Angle Convex Cone (SMACC) algorithm (Gruninger, Ratkowski, & Hoke, 2004). SMACC is an endmember extraction algorithm that also produces abundance maps of selected endmembers. The resulting maps show the amount of vegetation within each pixel from 0 (pure water, blue) to 100% (pure vegetation, red) for three different PRISM scenes (Fig. 11A–C). These mapped distributions were then used to conduct a spatial sensitivity analysis (Fig. 11D–F, see Section 3.4).

Two days after drifter deployment on 13 January, PRISM imagery revealed the initial seagrass debris as large amorphous wracks approximately 15 m by 100 m in size with low percent cover (Fig. 11A). Over the next day, debris aggregated bayside and formed defined windrows at distances of 5 to 15 m apart. Individual rows ranged in width from 1 m to 15 m and were several hundred meters in length (Fig. 11B). Finally, after winds shifted to a southerly direction, wrack was observed oceanside on 17 January. The wrack was concentrated into rows that were 18 to 35 m apart (Figs. 3A, 11C).

The abundance maps were used to assess the relationship between NIR reflectance and percent cover of seagrass. With near complete absorption of infrared radiation by pixels containing water alone and high reflectance by pixels with near 100% vegetative canopy, the magnitude of NIR reflectance should be a function of the amount of seagrass debris present within a pixel. A strong, nearly identical, relationship between estimated percent cover and average NIR reflectance (700–1050 nm) was observed for wracks from Days 3 and 5 (Fig. 12). The difference in the relationships was potentially related to seagrass debris ages. The higher slope in the older seagrass wrack was consistent with the

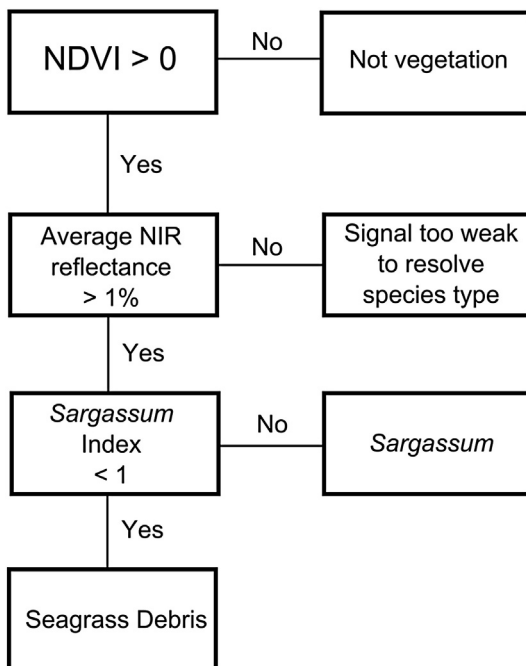


Fig. 6. A flowchart indicating the algorithm used to differentiate two types of floating vegetation found in this region: *Sargassum* and seagrass wrack.

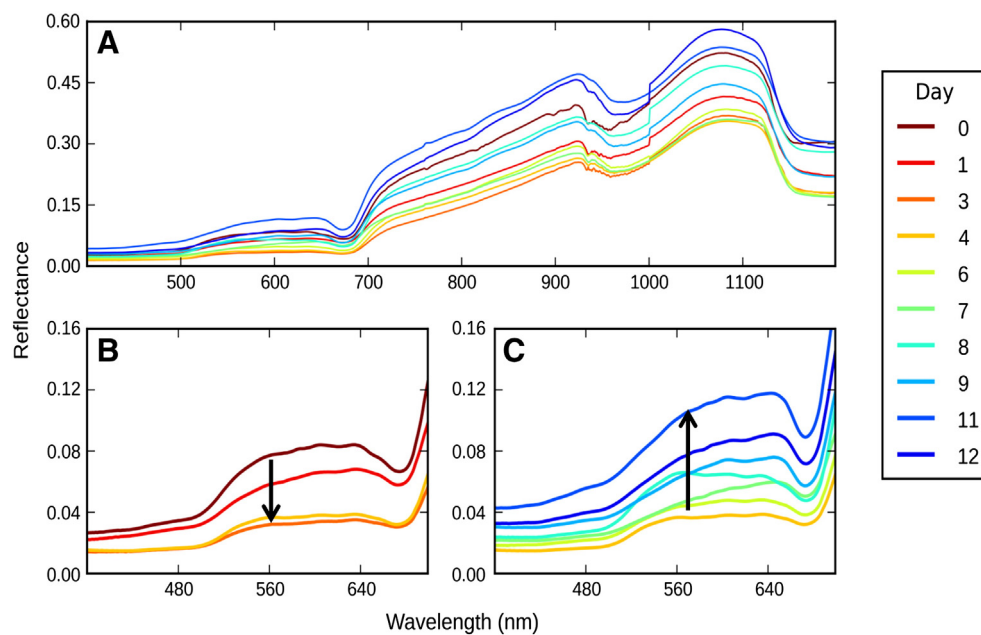


Fig. 7. A) Near-daily average reflectance measurements of *Syringodium* wrack taken from the mesocosm experiments show changes in spectral shape from Day 0 (blue) to Day 12 (black). The visible spectra for wrack aged B) 0 to 4 days and C) 4 to 12 days with arrows indicating the general change in reflectance over the indicated time period. (For interpretation of the references to color in this figure legend, the reader is referred to the web version of this article.)

mesocosm results showing increasing NIR reflectance with age. This approach could not be applied to the low density wrack detected on Day 2 due to the lack of pure pixels of seagrass in the imagery. The wrack had not aggregated into high enough concentrations and the seagrass was more dilute.

3.4. Analysis of spatial resolution

A limiting factor in detecting floating vegetation from space may be the spatial scales at which they form. The PRISM imagery resolved long narrow windrows of floating vegetation at 1 m resolution (Figs. 3A, 11B, C). Despite spanning long distances, however, the biomass in a given windrow only constitutes a small percent of a larger pixel due to the narrowness of the feature. Using the PRISM imagery, we assessed the ability for sensors like HypSIRI, with a nominal pixel size of 60 m, to identify seagrass at the scales observed during our field campaign. Because the wrack was not randomly distributed, we simulated a multitude of pixels ranging from 0 to 60 m in size with different

arrangements of seagrass wrack. Pixels were spatially aggregated by first randomly selecting 1000 1-m pixels containing floating vegetation from three 360 m × 360 m image subsets representing Days 2, 3 and 5 (Fig. 11). Each selected pixel within the image was incrementally increased in size from 1 to 60 m by averaging the reflectance measured in the surrounding pixels. At each pixel size, the reflectance was analyzed to determine whether seagrass debris was discernible from *Sargassum* using a threshold of 1% NIR reflectance. Fig. 11D–F shows the percentage of pixels in which seagrass debris was still discernible at each pixel size interval.

Results of spatial resolution analysis (Fig. 11D–F) indicated that seagrass debris was only detectable with 60 m pixels in a very few instances when wrack densities were high and individual windrows were within close proximity of one another. Specifically, the relationship was related to the size and shape of individual wracks, density of a wrack and proximity to other wracks. On Day 2 at a resolution of 1 m, approximately 75% of seagrass debris pixels were discernible (NIR > 0.01) from all floating vegetation (100% with NDVI > 0). Increasing pixel size to 5 m resulted in a sharp drop in detectable pixels followed by an increase and eventual decline to 0% detected at 41 m. When concentrated into windrows from 1 to 15 m, wrack was detectable 47% at 1 m and declined to 0.003% at a resolution of 60 m (Fig. 11E). Detectability was further reduced from 60% at 1 m for oceanside windrows to 0% at 13 m (Fig. 11F).

4. Discussion

Here, we show that different types of floating vegetation could be discriminated based on their hyperspectral signatures (Dierssen, 2013) and at different spatial resolutions.

4.1. Factors impacting the spectral properties

Spectral reflectance of the floating vegetation was quite variable in magnitude due to the degree of submergence in the water column. The spectra obtained on vegetation removed from the water were much higher across the visible and particularly the NIR than those taken in situ and from the imagery (see Fig. 4). This is largely because PRISM-imaged vegetation was floating at the air–water interface with

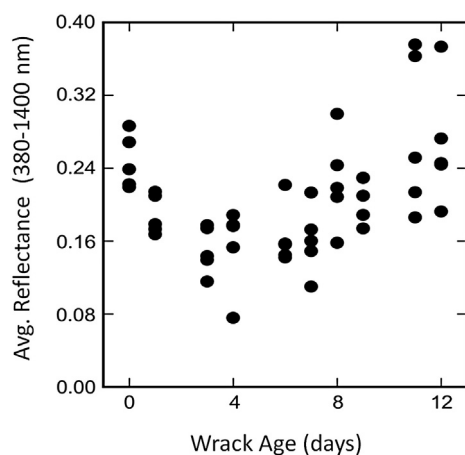


Fig. 8. Average reflectance across the visible and near infrared of *Syringodium* wrack in the mesocosms initially declined over 3 to 4 days and then increased for the remaining 8 days. Each dot represents one of five replicate reflectance measurements taken for each sample.

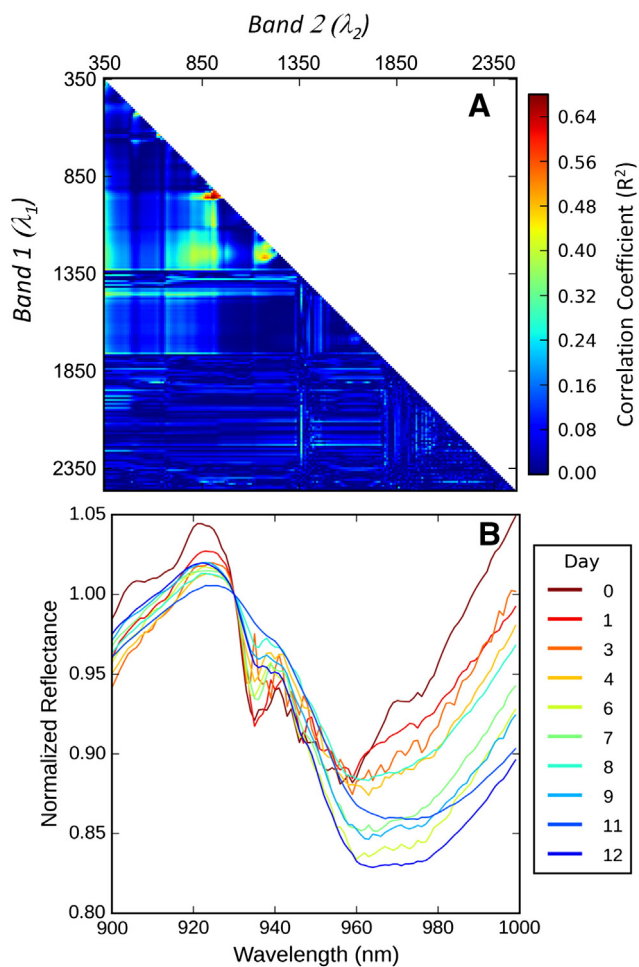


Fig. 9. A) Results of the narrowband pairwise index analysis of $NDVI_m$ calculated from measured wrack reflectances of two spectral bands (Eq. 1). Matrix color represents the correlation coefficient (R^2) for $NDVI_m$ and *Syringodium* wrack age. B) The measured wrack reflectance spectra in the spectral region with the highest correlation to wrack age from panel A.

both emergent and submerged parts. Photons reflecting off the submerged parts must pass through a layer of water which absorbs and scatters light depending on the optical properties of the water column. Natural water absorbs highly in red and NIR wavelengths (Smith & Baker, 1978) and phytoplankton and colored dissolved organic matter absorb in blue wavelengths (Dierssen & Randolph, 2013). As vegetation is submerged below the water surface, the spectra will get significantly lower in red and NIR to the point where the enhanced red edge reflectance produced by vegetation is completely absorbed by the water column. From airborne remote sensing, it is difficult to determine whether pixels with only a small NDVI signal occurred because of sparse vegetation, as modeled here, or because they are more deeply submerged in the water column (Marmorino et al., 2011).

Also, the age and location of the wrack played a role in the magnitude of reflectance and the amount of water signal mixed into the pixel. The wrack became more aggregated with higher abundance as the wrack aged. Select pixels within the imagery from Days 3 and 5 reflected pure endmembers with 100% wrack reflectance. Oceanside the wrack appeared in dense conglomerations (~300 g wet weight) of circular nested “whorls” that measured ~20 cm in diameter and ~10 cm in depth (Fig. 3B). On a 1 m pixel scale, spectral reflectance would be a mixture of 5–7 whorls with a few centimeters of water apparent between each whorl. Emergence of the vegetation above sea surface was also determined by whether it was free floating at the sea surface or compacted nearshore. Wrack found in the harbor, for

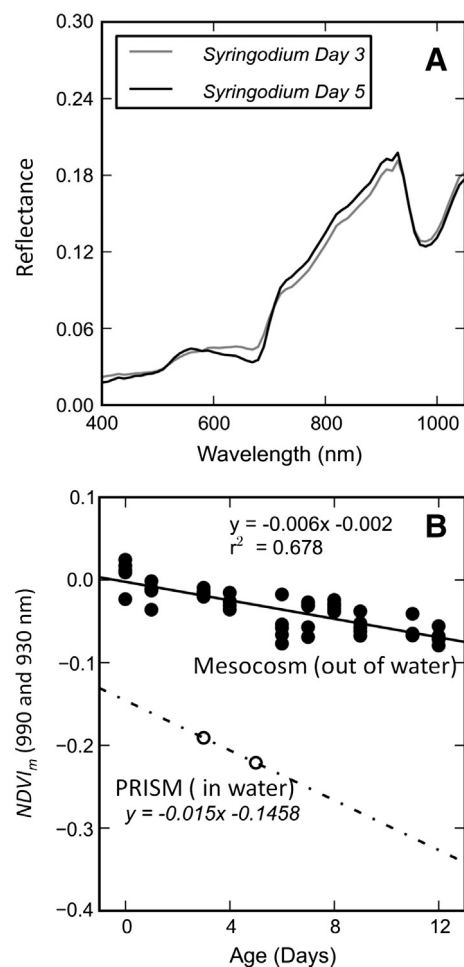


Fig. 10. A) Reflectance from pure *Syringodium* wrack endmembers derived from regions of the PRISM imagery associated with wrack of two different ages. B) Application of the $NDVI_m$ model using 930 and 990 nm applied to mesocosm data (black dots) and the two PRISM-derived endmembers from Panel A (white dots).

example, was tightly compressed and became nearly emergent with spectral characteristics approaching dry vegetation (e.g., Fig. 2).

While we have no direct validation of the age of the wrack present in the imagery, their location and estimated age were consistent with GPS drifter buoys released from the dense meadows that tracked surface water movement during the experiment. Although not concurrent with the overflight, one buoy advected oceanside was retrieved within a large patch of aggregated *Syringodium* wrack (Fig. 3B). Moreover, their spectral characteristics were consistent with aging experiments conducted in mesocosms at the laboratory. We had anticipated that the leaves would get browner and less reflective over time with chlorophyll loss and breakdown of cellular matter. Indeed such a pattern was observed initially over the course of 3–4 days in the mesocosms. However, the subsequent increase in reflectance from 5–12 days was reminiscent of typical leaf senescence in terrestrial ecosystems (Gitelson, Merzlyak, et al., 2003) and may also be due to the growth of a large epiphytic population of algae on the senescing leaves. The effect of declining chlorophyll content on reflectance spectra has been shown to initially affect wavelengths adjacent to the maximum chlorophyll absorption wavelength at 664 nm, between 530 and 630 nm and at 700 nm that can appear as an apparent chlorophyll absorption dip (Blackburn, 2007; Gitelson & Merzlyak, 1994). A rich population of photosynthetic epiphytes (Drake, Dobbs, & Zimmerman, 2003) was observed to grow on the leaves with a net increase in biomass over time. Because of this ambiguity, chlorophyll absorption was not a reliable method for assessing the age of the seagrass wrack.

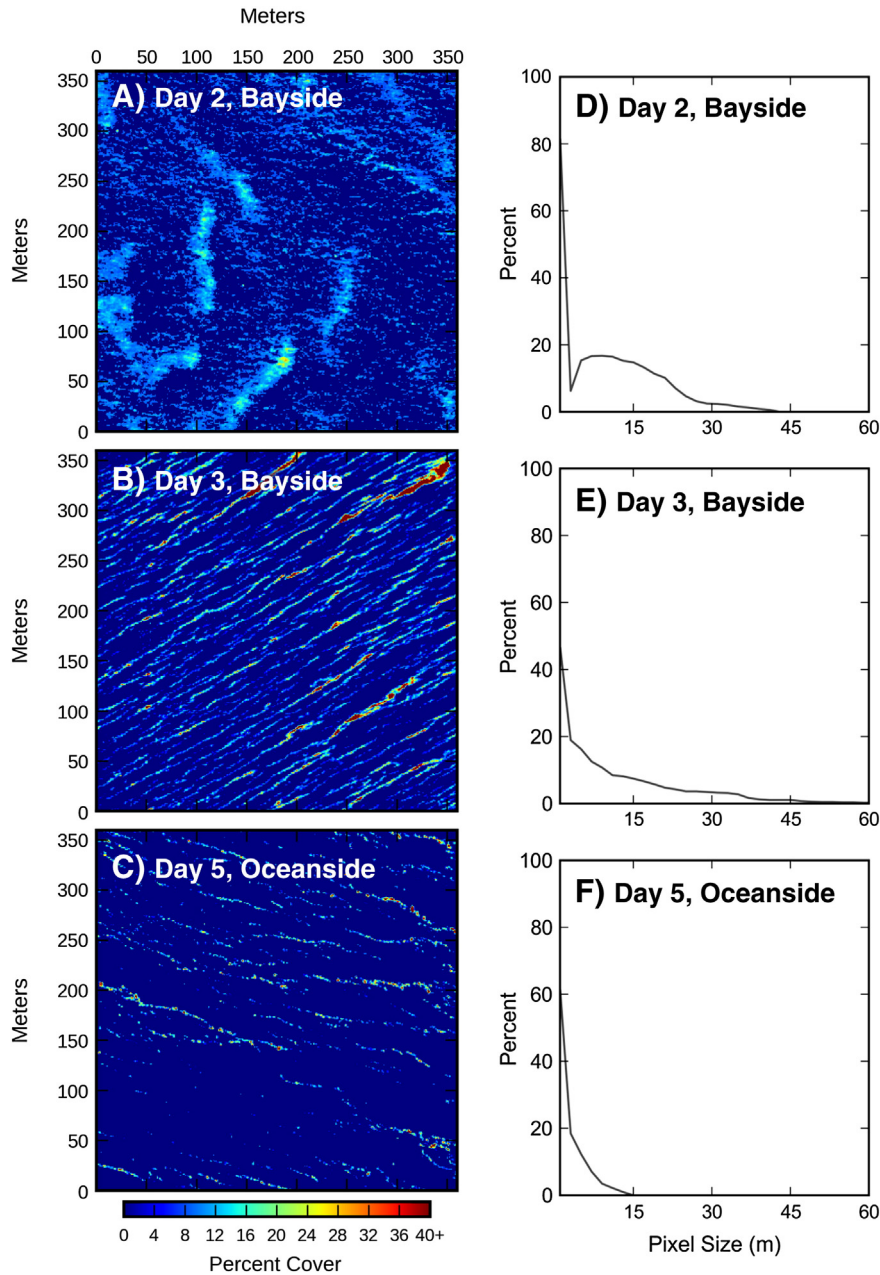


Fig. 11. A–C) Abundance of *Syringodium* wrack from three different portions of the PRISM imagery estimated as percent vegetation in a given pixel. Imagery reveals that the wrack became more aggregated over time. D–F) Results of the spatial sensitivity analysis to determine the percentage of *Syringodium* wrack that was detectable as pixel size increased from 1 to 60 m for each corresponding image in Column A.

Statistically, the best method for spectrally aging the wracks was with $NDVI_m$ using a narrow band water absorption feature at 990 nm (λ_1) compared to 930 nm (λ_2). These wavebands provided the highest correlation coefficient and are similar, but not identical, to those used for assessing water content in vegetation (900 and 970 nm). The water absorption feature centered around 970 nm (see Fig. 9B) is weak enough to allow the radiation to penetrate far into canopies and provide a larger dynamic range in water content (Claudio et al., 2006). Specifically, spectral reflectance of water-replete vegetation has a larger dip at these wavelengths compared to water-depleted vegetation. Here, the increasing absorption feature at 990 nm with increasing canopy age (i.e., more negative $NDVI_m$) indicates the presence of more water within the tissues over time. We hypothesize that cellular breakdown of the leaves and stems with age causes additional water content within the vegetation. Eventually, the intracellular water content may become great enough that biomass becomes negatively buoyant and sinks to

the seafloor. While the general trend in this feature was observed in the PRISM imagery, routine implementation of this algorithm may require alteration of the atmospheric correction routines that use short wave infrared bands (e.g., 980 nm) for sun glint correction.

4.2. Abundance and distribution of seagrass wrack

Our study focused on only one of the two commonly found seagrass species in this region – the cylindrical-bladed manatee grass or *Syringodium filiforme*. This species forms dense meadows in Greater Florida Bay (Frankovich et al., 2009; McPherson et al., 2011) and contributed to over 97% of the wrack by wet weight observed during our study. Past studies suggest that 50–70% of the carbon produced from this species is exported out of the beds (Mateo, Cebrian, Dunton, & Mutchler, 2006). Export rates from the other common seagrass, *Thalassia testudinum*, varied widely in the literature from 1–48%

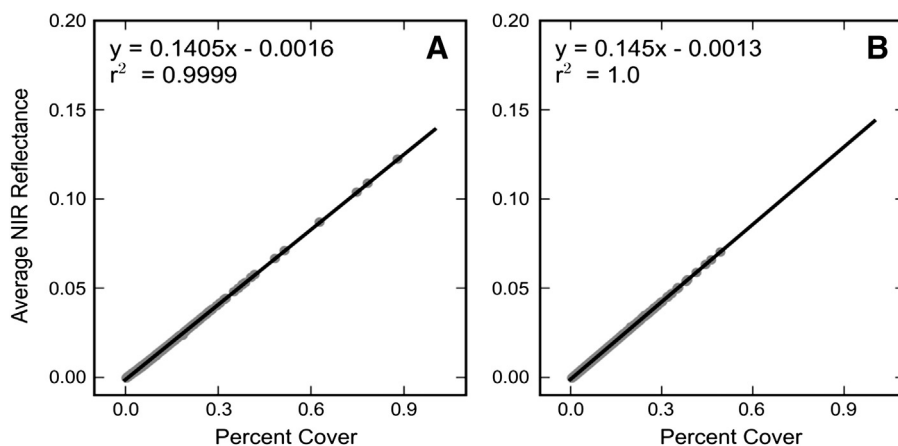


Fig. 12. The relationship between estimated percent cover and average NIR reflectance (700–1050 nm) for *Syringodium* wracks from A) Day 3 and B) Day 5.

(Mateo et al., 2006), but little *Thalassia* leaf litter was observed at the sea surface during our study (<3%). Production of leaf litter is a continual process for healthy growth of seagrass where one leaf on a shoot is added and the most mature leaf is shed. Turnover rates can vary from weeks to months depending on the species (Hemminga & Duarte, 2000).

High amounts of wrack can also be produced during high wind events that cause turbulence along the seafloor. Our study occurred in winter months with periodic high wind speeds over 10 m s^{-1} . Buoy studies showed that flow generally followed the tidal patterns within Greater Florida Bay that would keep debris bayside. However, when wind directions became southerly, the drifters were advected through tidal channels between the islands and biomass was exported from bayside to oceanside.

Over time the leaf debris became more aggregated due to circulation patterns primarily driven by winds and tides bayside and also by the larger Gulf Stream fronts on the oceanside (Haney & McGillivray, 1985). Initially individual leaves could be observed floating in isolation away from the seagrass meadows. Leaf debris aggregated first in the shallow bayside waters (Day 3) in ~10 m rows and then in more separated ~30 m rows oceanside (Day 5). Aggregated rows of vegetation are commonly found in shallow waters due to three-dimensional rotating cells that form surface convergence at the boundary of counter-rotating cells called “Langmuir circulation” (Faller, 1971). Langmuir cells at scales of 2 m to 1 km occur from the interaction of the Stokes drift induced by surface waves and the vertical shear in turbulent fluid (Thorpe, 2004). Langmuir circulation is commonly observed as windrows of buoyant material including algae, plankton, or bubbles aligned parallel to the winds (Monahan & Lu, 1990). Langmuir cells that reach the full depth of the water column, Langmuir “supercells,” have been observed to concentrate macroalgae on the seafloor (Dierssen, Zimmerman, Drake, et al., 2009) and can produce sediment resuspensions (Dierssen, Zimmerman & Burdige, 2009; Gargett, Wells, Tejada-Martinez, & Grosch, 2004). At the sea surface, aggregations are observed on the downwelling interface between cells and the width of the rows depends primarily on wind speed and the water depth.

Seagrass wrack abundance was calculated using predefined thresholds. An NDVI threshold greater than 0 was used to indicate the presence of floating vegetation with enhanced NIR reflectance. However, a higher abundance of floating vegetation was required to differentiate the type of vegetation. An NIR reflectance of 1% was considered sufficient to differentiate between *Syringodium* wrack and *Sargassum*. This threshold can vary with water properties and whether the water is considered optically shallow whereby reflectance from the seafloor contributes to water leaving radiance at the sea surface (Dekker et al., 2011).

Whether these NDVI thresholds can be universally applied to other regions and vegetation types remains to be seen. An NDVI threshold

was used to differentiate the presence of submerged and emergent vegetation in Floridian waters of St. Joseph Bay (Hill, Zimmerman, Bissett, Dierssen, & Kohler, 2014). The abundance of the giant kelp *Macrocystis pyrifera* was also estimated using satellite-derived estimates of NDVI (Cavanaugh et al., 2010). Enhanced NDVI may also be the result of densely concentrated phytoplankton at the sea surface. Cyanobacterial blooms, for example, can be detected due to enhancements in backscatter near the red edge reflectance (Matthews, Bernard, & Robertson, 2012). With the push towards more hyperspectral imagery, however, specific narrowband indices can aid in identification of unknown sources of enhanced NIR reflectance in oceanic waters. The presence of floating vegetation may be detected using multi-spectral imagery, but higher spectral resolution imagery (10 nm) was necessary to distinguish between these two types of vegetation.

4.3. Implications for remote sensing

The results of this study show that remote sensing can be used to assess different types of floating vegetation with appropriate spectral and spatial resolution imagery. Airborne remote sensing with the PRISM sensor was highly effective at assessing the fine-scale aggregations of seagrass wrack that could not be easily observed from satellites. Langmuir circulation is often studied with point measurements that show cyclical temporal patterns of physical and optical parameters (Gargett et al., 2004), but airborne remote sensing can be used to view these patterns on the sea surface directly with orientation and expanse of the windrows clearly illuminated. As expected, the average width of the windrows was related to the water depth with closer rows in shallow bayside and further spaced rows in deeper shelf waters. Such patterns are challenging to visualize without remote sensing technology. While not the focus of this study directly, convergent features and structures found on the sea surface play important roles in ecology, oceanography, and climatology (Klemas, 2011).

This is one of the first studies to differentiate types of floating vegetation beyond generalized enhancements in NIR reflectance. In vast expanses of the subtropical oligotrophic ocean, the presence of enhanced NIR reflectance is likely to be due to drifting *Sargassum* macroalgae. In coastal regions like the Yellow Sea (Hu & He, 2008) or Greater Florida Bay, however, the source of floating vegetation is not well constrained. Here, we show that *Sargassum* can be differentiated from seagrass wrack with hyperspectral imagery based on the “spectral fingerprint” of *Sargassum*. Such differentiations can be important in understanding the biogeochemistry of the region. Ecologically, the role played by pelagic *Sargassum*, a living, photosynthesizing macroalgae with a persistent faunal community, is quite different from ephemeral floating leaf and stem debris. Seagrass wrack serves to export carbon and associated nutrients out of the seagrass meadow and eventually lands on shore or

sinks to the seafloor (Heck et al., 2008; Mateo et al., 2006). For some types of seagrasses, a large fraction of carbon is thought to be recycled within the meadow and sediments, a source of recycled “blue” carbon and potentially carbonate dissolution (Burdige, Hu, & Zimmerman, 2008; Mcleod et al., 2011). This study suggests that remote sensing technology can be used to assess the exported flux of carbon out of seagrass meadows comprised of different seagrass species.

Coastal residents are aware that significant amounts of wrack from both *Sargassum* and seagrass wash ashore into harbors and onto beaches. From an economic perspective, remote sensing technology can help forecast when coastal cleanup efforts may be required. For such applications, assessing the type of floating vegetation may not be as important as the frequency and extent of the floating biomass. Hence, spectral resolution may be sacrificed for higher spatial and temporal resolution imagery. Certainly, the ephemeral nature of the vegetation and linkages to episodic high wind speed events suggest that sensors with frequent revisit times and high spatial resolution, like airborne PRISM overflights, would be necessary for effective coastal monitoring. Further development of technology and methods for high spectral, spatial, and temporal resolution hyperspectral imagery will be useful not only for differentiating types of floating vegetation from an ecological and biogeochemical perspective, but for monitoring programs that assess coastal health and resilience.

Acknowledgments

This research was primarily funded by the National Aeronautics and Space Administration (NASA) Ocean Biology and Biogeochemistry Program (NNX13AH88G). Additional funding for the PRISM instrument has been provided by NASA's Earth Science and Technology Office, and the Airborne Science programs. We wish to acknowledge Bo-Cai Gao at the Naval Research Laboratory and the PRISM team at NASA Jet Propulsion Laboratories including P. Mouroulis, R. Greene, B. VanGorp, I. McCubbin, and D. Thompson for their assistance in obtaining and processing the PRISM imagery. We wish to thank Rachel Perry, Jeff Godfrey, and Ninoshka De Jesus Rivera from the University of Connecticut for assistance in data collection and the staff at Keys Marine Laboratory for providing facilities and vessel support for our experiments.

References

- Beach, K. S., Borgeas, H. B., Nishimura, N. J., & Smith, C. M. (1997). In vivo absorbance spectra and the ecophysiology of reef macroalgae. *Coral Reefs*, 16, 21–28.
- Blackburn, G. A. (2007). Hyperspectral remote sensing of plant pigments. *Journal of Experimental Botany*, 58, 855–867.
- Burdige, D. J., Hu, X., & Zimmerman, R. C. (2008). Rates of carbonate dissolution in permeable sediments estimated from pore water profiles: The role of seagrasses. *Limnology and Oceanography*, 53, 549–565.
- Cavanaugh, K. C., Siegel, D. A., Kinlan, B. P., & Reed, D. C. (2010). Scaling giant kelp field measurements to regional scales using satellite observations. *Marine Ecology Progress Series*, 403, 13–27.
- Claudio, H. C., Cheng, Y., Fuentes, D. A., Gamon, J. A., Luo, H., Oechel, W., et al. (2006). Monitoring drought effects on vegetation water content and fluxes in chaparral with the 970 nm water band index. *Remote Sensing of Environment*, 103, 304–311.
- Connolly, K. D. (2002). *Introduction to the essential fish habitat (EFH) consultation process for the south Atlantic region*. An. Se Emtl LJ 11, 1.
- Coston-Clements, L., & Center, S. F. (1991). *Utilization of the Sargassum habitat by marine invertebrates and vertebrates: A review*. US Department of Commerce, National Oceanic and Atmospheric Administration, National Marine Fisheries Service, Southeast Fisheries Science Center, Beaufort Laboratory.
- Cummings, M. E., & Zimmerman, R. C. (2003). Light harvesting and the package effect in the seagrasses *Thalassia testudinum* Banks ex König and *Zostera marina* L.: Optical constraints on photoacclimation. *Aquatic Botany*, 75, 261–274.
- Dekker, A. G., Phinn, S. R., Anstee, J., Bissett, P., Brando, V. E., Casey, B., et al. (2011). Intercomparison of shallow water bathymetry, hydro-optics, and benthos mapping techniques in Australian and Caribbean coastal environments. *Limnology and Oceanography: Methods*, 9, 396–425.
- Dierssen, H. M. (2013). *Overview of hyperspectral remote sensing for mapping marine benthic habitats from airborne and underwater sensors*. Imaging Spectrometry XVIII. Proc of SPIE, 1–7.
- Dierssen, H. M., Kudela, R. M., Ryan, J. P., & Zimmerman, R. C. (2006). Red and black tides: Quantitative analysis of water-leaving radiance and perceived color for phytoplankton, colored dissolved organic matter, and suspended sediments. *Limnology and Oceanography*, 51, 2646–2659.
- Dierssen, H. M., & Randolph, K. (2013). Remote sensing of ocean color. *Encyclopedia of sustainability science and technology* (pp. 25). Springer-Verlag.
- Dierssen, H. M., Zimmerman, R. C., & Burdige, D. J. (2009). Optics and remote sensing of Bahamian carbonate sediment whittings and potential relationship to wind-driven Langmuir circulation. *Biogeosciences*, 6, 487–500.
- Dierssen, H. M., Zimmerman, R. C., Drake, L. A., & Burdige, D. J. (2009). Potential export of unattached benthic macroalgae to the deep sea through wind-driven Langmuir circulation. *Geophysical Research Letters*, 36, L04602.
- Drake, L. A., Dobbs, F. C., & Zimmerman, R. C. (2003). Effects of epiphyte load on optical properties and photosynthetic potential of the seagrasses *Thalassia testudinum* Banks ex König and *Zostera marina* L. *Limnology and Oceanography*, 48, 456–463.
- Dugan, J. E., Hubbard, D. M., McCrary, M. D., & Pierson, M. O. (2003). The response of macrofauna communities and shorebirds to macrophyte wrack subsidies on exposed sandy beaches of southern California. *Estuarine, Coastal and Shelf Science*, 58, 25–40.
- Faller, A. J. (1971). Oceanic turbulence and the Langmuir circulations. *Annual Review of Ecology and Systematics*, 2, 201–236.
- Fourqurean, J. W., Willisie, A., Rose, C. D., & Rutten, L. M. (2001). Spatial and temporal pattern in seagrass community composition and productivity in south Florida. *Marine Biology*, 138, 341–354.
- Frankovich, T. A., Armitage, A. R., Wachnicka, A. H., Gaiser, E. E., & Fourqurean, J. W. (2009). Nutrient effects on seagrass epiphyte community structure in Florida Bay. *Journal of Phycology*, 45, 1010–1020.
- Gao, B. -C., & Davis, C. O. (1997). *Development of a line-by-line-based atmosphere removal algorithm for airborne and spaceborne imaging spectrometers*. Optical Science, Engineering and Instrumentation '97. International Society for Optics and Photonics, 132–141.
- Gargett, A. E., Wells, J. R., Tejada-Martinez, A. E., & Grosch, C. E. (2004). Langmuir supercells: A mechanism for sediment resuspension and transport in shallow seas. *Science*, 306, 1925–1927.
- Gitelson, A., & Merzlyak, M. N. (1994). Spectral reflectance changes associated with Autumn senescence of *Aesculus hippocastanum* L. and *Acer platanoides* L. leaves. *Journal of Plant Physiology*, 143, 286–292.
- Gitelson, A. A., Merzlyak, M. N., et al. (2003). Relationships between leaf chlorophyll content and spectral reflectance and algorithms for non-destructive chlorophyll assessment in higher plant leaves. *Journal of Plant Physiology*, 160, 271–282.
- Gower, J., Hu, C., Borstad, G., & King, S. (2006). Ocean color satellites show extensive lines of floating *Sargassum* in the Gulf of Mexico. *Geoscience and Remote Sensing, IEEE Transactions on*, 44, 3619–3625.
- Gower, J., King, S., Borstad, G., & Brown, L. (2008). The importance of a band at 709 nm for interpreting water-leaving spectral radiance. *Canadian Journal of Remote Sensing*, 34, 287–295.
- Gruninger, J. H., Ratkowski, A. J., & Hoke, M. L. (2004). *The sequential maximum angle convex cone (SMACC) endmember model*. Defense and Security. International Society for Optics and Photonics, 1–14.
- Grzymiski, J., Johnsen, G., & Sakshaug, E. (1997). The significance of intracellular self-shading on the biooptical properties of brown, red, and green macroalgae. *Journal of Phycology*, 33, 408–414.
- Haney, J. C., & McGillivray, P. A. (1985). Aggregations of Cory's shearwaters (*Calonectris diomedea*) at Gulf Stream fronts. *Wilson Bulletin*, 191–200.
- Heck, K. L., Jr., Carruthers, T. J., Duarte, C. M., Hughes, A. R., Kendrick, G., Orth, R. J., et al. (2008). Trophic transfers from seagrass meadows subsidize diverse marine and terrestrial consumers. *Ecosystems*, 11, 1198–1210.
- Hemminga, M., & Duarte, C. (2000). *Seagrass ecology*. Cambridge University Press.
- Herron, R. C., Leming, T. D., & Li, J. (1989). Satellite-detected fronts and butterflyfish aggregations in the northeastern Gulf of Mexico. *Continental Shelf Research*, 9, 569–588.
- Hill, V. J., Zimmerman, R. C., Bissett, W. P., Dierssen, H., & Kohler, D. D. (2014). Evaluating light availability, seagrass biomass, and productivity using hyperspectral airborne remote sensing in Saint Joseph's Bay, Florida. *Estuaries and Coasts*, 1–23.
- Hu, C. (2009). A novel ocean color index to detect floating algae in the global oceans. *Remote Sensing of Environment*, 113, 2118–2129.
- Hu, C., & He, M. -X. (2008). Origin and offshore extent of floating algae in Olympic sailing area. *Eos, Transactions of the American Geophysical Union*, 89, 302–303.
- Ince, R., Hyndes, G. A., Lavery, P. S., & Vanderklift, M. A. (2007). Marine macrophytes directly enhance abundances of sandy beach fauna through provision of food and habitat. *Estuarine, Coastal and Shelf Science*, 74, 77–86.
- Johnsen, G., & Sakshaug, E. (2007). Biooptical characteristics of PSII and PSI in 33 species (13 pigment groups) of marine phytoplankton, and the relevance for pulse-amplitude-modulated and fast-repetition-rate fluorometry1. *Journal of Phycology*, 43, 1236–1251.
- Jordan, C. F. (1969). Derivation of leaf-area index from quality of light on the forest floor. *Ecology*, 663–666.
- Klemas, V. (2011). Remote sensing of coastal plumes and ocean fronts: Overview and case study. *Journal of Coastal Research*, 28, 1–7.
- Lavery, P. S., McMahon, K., Weyers, J., Boyce, M. C., & Oldham, C. E. (2013). Release of dissolved organic carbon from seagrass wrack and its implications for trophic connectivity. *Marine Ecology Progress Series*, 494, 121–133.
- Macreadie, P. I., Hughes, A. R., & Kimbro, D. L. (2013). Loss of “blue carbon” from coastal salt marshes following habitat disturbance. *PLoS One*, 8, e69244.
- Marmorino, G. O., Miller, W. D., Smith, G. B., & Bowles, J. H. (2011). Airborne imagery of a disintegrating *Sargassum* drift line. *Deep Sea Research Part I: Oceanographic Research Papers*, 58, 316–321.
- Mateo, M. A., Cebrian, J., Dunton, K., & Mutchler, T. (2006). Carbon flux in seagrasses. *Seagrasses: Biology, ecology, and conservation* (pp. 159–192). Springer.

- Matthews, M. W., Bernard, S., & Robertson, L. (2012). An algorithm for detecting trophic status (chlorophyll-*a*), cyanobacterial-dominance, surface scums and floating vegetation in inland and coastal waters. *Remote Sensing of Environment*, *124*, 637–652.
- Mcleod, E., Chmura, G. L., Bouillon, S., Salm, R., Björk, M., Duarte, C. M., et al. (2011). A blueprint for blue carbon: Toward an improved understanding of the role of vegetated coastal habitats in sequestering CO₂. *Frontiers in Ecology and the Environment*, *9*, 552–560.
- McPherson, M. L., Hill, V. J., Zimmerman, R. C., & Dierssen, H. M. (2011). The optical properties of Greater Florida Bay: Implications for seagrass abundance. *Estuaries and Coasts*, 1–11.
- Mellbrand, K., Lavery, P. S., Hyndes, G., & Hambäck, P. A. (2011). Linking land and sea: Different pathways for marine subsidies. *Ecosystems*, *14*, 732–744.
- Mobley, C. D. (1999). Estimation of the remote sensing reflectance from above-surface measurements. *Applied Optics*, *38*, 7442–7455.
- Monahan, E. C., & Lu, M. (1990). Acoustically relevant bubble assemblages and their dependence on meteorological parameters. *IEEE Journal of Oceanic Engineering*, *15*, 340–349.
- Mossbauer, M., Haller, I., Dahlke, S., & Schernewski, G. (2012). Management of stranded eelgrass and macroalgae along the German Baltic coastline. *Ocean and Coastal Management*, *57*, 1–9.
- Mouroulis, P., Green, R. O., & Wilson, D. W. (2008). Optical design of a coastal ocean imaging spectrometer. *Optics Express*, *16*, 9087–9096.
- Mouroulis, P., Van Gorp, B., Green, R. O., Dierssen, H., Wilson, D. W., Eastwood, M., et al. (2013). *The Portable Remote Imaging Spectrometer (PRISM) coastal ocean sensor: Design, characteristics and first flight results.*
- Mutanga, O., & Skidmore, A. K. (2004). Narrow band vegetation indices overcome the saturation problem in biomass estimation. *International Journal of Remote Sensing*, *25*, 3999–4014.
- Oldham, C. E., Lavery, P. S., McMahon, K., Pattiaratchi, C., & Chiffings, T. (2010). *Seagrass wrack dynamics in Geopraphe Bay, Western Australia.* Department of Transport, Shire of Busselton.
- Peñuelas, J., Pinol, J., Ogaya, R., & Filella, I. (1997). Estimation of plant water concentration by the reflectance water index WI (R900/R970). *International Journal of Remote Sensing*, *18*, 2869–2875.
- Smith, R. C., & Baker, K. S. (1978). Optical classification of natural waters. *Limnology and Oceanography*, *23*, 260–267.
- Szekielda, K. H., Marmorino, G. O., Bowles, J. H., & Gillis, D. (2010). High spatial resolution spectrometry of rafting macroalgae (*Sargassum*). *Journal of Applied Remote Sensing*, *4* (043529–043529).
- Thorpe, S. A. (2004). Langmuir circulation. *Annual Review of Fluid Mechanics*, *36*, 55–79.
- Tucker, C. J. (1979). Red and photographic infrared linear combinations for monitoring vegetation. *Remote Sensing of Environment*, *8*, 127–150.
- Webster, R. K., & Linton, T. (2013). Development and implementation of *Sargassum* Early Advisory System (SEAS). *Shore & Beach*, *81*, 1.
- Witherington, B. (2002). Ecology of neonate loggerhead turtles inhabiting lines of downwelling near a Gulf Stream front. *Marine Biology*, *140*, 843–853.